

DOI:

Towards an efficient and robust numerical strategy for fast aerodynamic performance prediction on launch vehicles

P. E. Weiss^{†} and S. Deck^{*}*

^{} ONERA - The French Aerospace Lab, F-92190, Meudon, France
peweiss@onera.fr · sebastien.deck@onera.fr*

[†]Corresponding author

Abstract

The present work aims at increasing the responsiveness of aerodynamic coefficient predictions for the investigation of the effects of technological details. Starting from a simplified configuration and using Zonal Immersed Boundary Conditions¹⁸ which combine the local use of both a modelling method (e.g. RANS, URANS, ZDES, LES or DNS) and IBC (Immersed Boundary Conditions), realistic configurations^{12,20,24,31} are rapidly turned into feasible numerical simulations.^{30,32} In this paper, the efficiency and the robustness of the methodology is demonstrated using a simplified Ariane 5 configuration discretized with a body-fitted approach. Then, the effect of additional protrusions on the flow is mimicked thanks to Zonal Immersed Boundary Conditions allowing to simulate a complete Ariane 5 space launcher configuration along with the sting holding the model. The unsteady side-loads are compared with the available experimental data.

1. Introduction

Considering the current level of maturity of advanced turbulent modelling methods (see e.g.^{2,3,22,27}), the ability to establish a global strategy for a fast prediction of the aerodynamic performance based on well-defined and easily reproducible milestones to tackle the geometrical complexity becomes a topic of growing interest.

The methodology is explicated in a step-by-step manner which summarizes the detailed description proposed in Weiss and Deck.³² The present investigation exhibits the instantaneous flow fields and time-averaged data such as the statistical moments of the pressure coefficients for a qualitative and quantitative analysis, respectively. Finally, the discussion ends with an analysis of the spectral content leading the dynamics of the fluctuating flow field as in Weiss and Deck²⁸ or Pain *et al.*²⁰ The results are thoroughly compared to the available dataset from NLR's experiments conducted in the framework of ESA's TRP (Hannemann *et al.*,¹² Schwane²⁴).

2. Test case

A full Ariane 5 model with a 1:60 subscale ratio is modelled along with the Z-shape sting holding the model in NLR's experiments^{9,10,24} performed in the DNW-HST facility for representativeness purposes. The flow around this complex geometry is computed at a high Reynolds number $Re_D = 1.18 \times 10^6$ based on the largest cylinder diameter D of the main stage and for a freestream Mach number $M_\infty = 0.8$. This well-documented test case with NLR's steady tabs and unsteady Kulites permits to validate the computed values of relevant physical quantities such as the mean and fluctuating pressure coefficients in the flow field and at the wall, characterizing the interaction between the recirculation bubbles and the multiple shear layers.

3. Global strategy for a fast prediction of the aerodynamic performance

3.1 Milestones of an efficient ZIBC simulation design

A key feature of the automation of the aerodynamic performance prediction is the capability to define simple reproducible steps which can be easily adapted on demand. Such a procedure is described in detail in Weiss and Deck³² and summarized hereafter:

TOWARDS AN EFFICIENT AND ROBUST NUMERICAL STRATEGY FOR FAST AERODYNAMIC PERFORMANCE PREDICTION ON LAUNCH VEHICLES

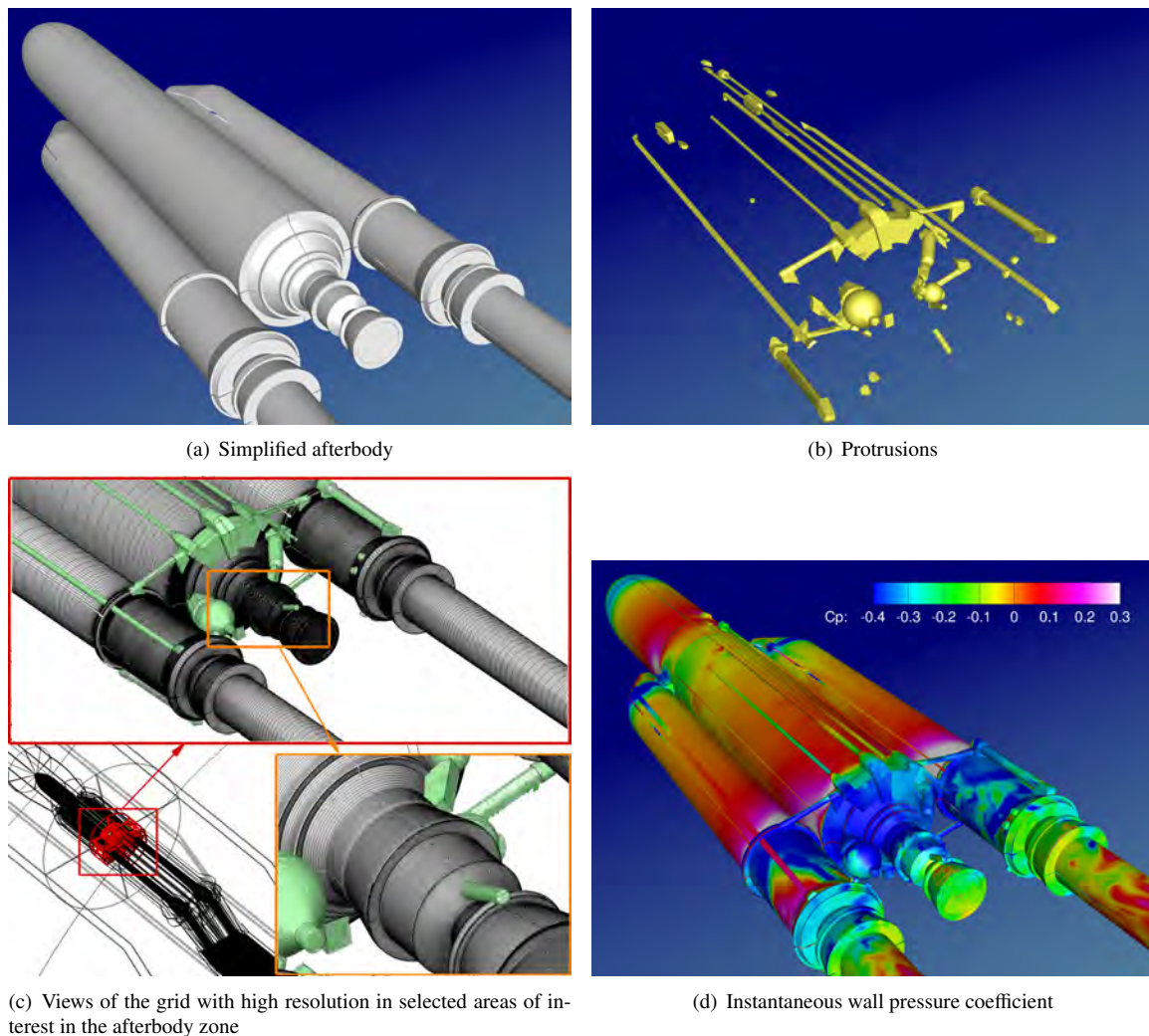


Figure 1: Example of the numerical strategy for the taking into account of Ariane 5's technological details

1. CAD file(s) without technological details (see figure 1(a))
2. Mesh with high resolution in selected area(s) of interest (see figure 1(c))
3. CAD file(s) for technological details (see figure 1(b))
4. Tagging procedure to immerse the technological details whose effect is to be assessed in the selected highly refined areas of interest
5. Run numerical simulation with ZIBC formulation (numerical approach (here ZDES mode 2) + IBC)
6. Gather wall quantities from both the classical no-slip boundary conditions along with the values issuing from the projection on IB bodies
7. Visualization of instantaneous and time-averaged flow fields
8. Plot of integrated loads to quantify the aerodynamic performance in the area(s) of interest
9. Redo from step 3 with different CAD files of other protuberances to quickly evidence the differences between two configurations regarding the aerodynamic force and torque

3.2 Grid

The computational domain is made up with an O-H topology to avoid singularity problems near the axis of the axisymmetric bodies. The mesh contains 164 structured blocks and a total number of 75×10^6 points with an azimuthal resolution on the central part of the afterbody corresponding to $\Delta\Phi = 1^\circ$. A body-fitted mesh of the so-called ‘clean configuration’¹⁰ is obtained and consists in a smooth representation of the boosters and the main stage. The highest refined area is located in the afterbody zone clustering approximately two-thirds of the total number of grid points and fitting LES requirements. In particular, the early stages of the shear layers and the braids linking the pairing vortices are discretized with 15 points²⁵ and at least 7 points,¹³ respectively. Such a resolution allows an accurate representation of the several technological details (e.g. DAAR ring, asymmetric struts, helium sphere, etc.)^{12,20,24,31} after the tagging procedure which constitutes the preliminary step to use immersed boundary conditions.

3.3 Numerical set up

The ZIBC strategy whose formulation is explicated in Weiss and Deck³² is based on the original IB method using direct forcing^{8,19} and on the ZDES approach.^{4,5} We have implemented the original IB method in two industrial flow solvers namely FLU3M¹¹ and ONERA’s elsA software.² Both codes are based on second-order accurate time and space schemes. The calculations presented in this paper are performed with the FLU3M code. This code solves the Navier-Stokes equations with a low-dissipation AUSM+(P) convective scheme¹⁴ on multiblock structured grids. The time integration is carried out by means of an implicit second-order accurate backward scheme. Time accuracy of the calculation was checked during the inner iteration process.^{17,21} The simulation was performed on 256 Nehalem X5560 cores (1 Nehalem node being made of 2 quad-core processors). The CPU cost per cell and per inner-iteration is about 3×10^{-6} s. The preprocessing needed by the IBC to distinguish mesh cells with a fluid or solid tag is realized by the external program RAYTRACER3D¹⁸ and the Cassiopée modules¹ for FLU3M and elsA, respectively.

4. Results: post-processing and analysis steps

4.1 Step 1: identification of the main instantaneous and statistical features of the flow

The qualitative analysis of the spatial organization of the coherent structures in the afterbody area allows to evidence the salient features of the flow dynamics. In figure 2 several views of a Q criterion iso-surface coloured by the streamwise component of the vorticity and the velocity are represented. The sole structures of the area of interest namely the afterbody of the main stage (EPC) are considered given the total amount of cells of the mesh (i.e. $N_{xyz} = 75 \times 10^6$) does not permit to properly model the flow dynamics around the boosters (EAP). To do so, a grid containing at least 120×10^6 points would have been necessary.³¹ However, the present study does not focus on the influence of the flow between the EAPs and the EPC.

Large scale structures are observed due to the presence of the struts showing the IBC approach is efficient to model these technological details which are well-taken into account in the numerical simulation. These coherent structures amplify the pairing process of the axisymmetric mixing layer as observed on the contour plots of the density gradient norm represented in figure 2 which permits to evidence the spatial evolution of pressure waves in the flow. The wall signature characteristic of the impact of the coherent structures on the afterbody surface are distributed on the EAPs and the EPC. The cut planes in the non-booster plane (NB) show the formation of large scale structures in the mixing layer issuing from the separation near the main stage upstream cylinder. Similar phenomena are noticed in the instantaneous and mean fields of the dimensionless streamwise velocity (cf. figure 3) and of the backflow area (cf. figure 5).

A qualitative analysis of the instantaneous streamwise velocity field allows to notice a quasi-zero-mass-flow area in the booster plane (B). In plane (NB) of the launcher, the velocity field shown in figure 3 is very close to the one observed around a simple axisymmetric backward facing step of finite length (see^{7,15,16,23,26,29,33}) in the transonic regime. Indeed, in plane (NB), a mixing layer develops and surrounds a primary recirculation zone on the extension of the EPC for both cases. Then, a secondary recirculation zone is observed downstream of the nozzle. In plane (B), jets occur near the asymmetric struts deflected by coanda effect to the boosters as assumed and explained by Pain *et al.*²⁰ Finally, areas displaying a backflow are circumscribed by the iso-surface for the zero streamwise velocity represented in figure 5. Such a representation permits to evidence a clear asymmetry of the recirculation zone in the afterbody

region.

Figures 6, 7 and 8 illustrate the pressure coefficient C_p , the dimensionless streamwise velocity u/U_∞ and the density gradient norm $\|\overrightarrow{grad\rho}\|$ in $(y-z)$ planes which are normal to the main flow direction and equally distributed along the extension of the central part of the afterbody (plane $P1$ to plane $P9$) and downstream the nozzle (plane $P10$). One can note that the struts strongly impact the instantaneous azimuthal topology of the flow close to the separation on the largest cylinder of the main stage. The other protrusions appear to be of lesser influence on the flow dynamics in the azimuthal direction and further in the wake. The streamwise velocity field of figures 7 show that the order of magnitude of the backflow is from 20% to 30% of the freestream velocity value. A salient asymmetry is observed in the wake at locations $x/D = 1.05$ and 1.35 .

These qualitative analyses suggest that the technological details leading to a macroscopic change in the global spatial organization of the aerodynamic field are the asymmetric struts linking the main stage to the boosters.

This phenomenon could be at the origin of the non-symmetric bi-lobe shape of the wall pressure coefficient contours on the nozzle divergent of the main stage observed in the views of the instantaneous field in figure 1(d) and the mean field in figure 4.

In the same spirit, figure 4 depicts the distribution of the mean and fluctuating pressure at the wall and in the flow field. The streamwise evolution for a given azimuthal location of the *rms* pressure values in the vicinity of the axisymmetric shear layer developing around the main stage in the afterbody region varies a lot depending on the considered azimuthal plane. Then, LOX and LH2 pressurization lines upstream from the separation at the end of the largest cylinder of the main stage directly influence the fluctuating pressure levels (cf. figure 4), reminding the effect on the aerodynamic field around the skirt control devices tested at NLR.¹⁰

4.2 Step 2: evidence of the side-load origin

The time average of the streamwise velocity field plotted in figure 3 in the booster (B) and non-booster (NB) planes permits to appreciate the mean topology of the flow. The primary recirculation zone extends until the middle of the nozzle in plane (B) but is limited to the first half part of the extension in plane (NB). The mean tridimensional view (see the lower part of figure 5) illustrates the azimuthal evolution generating this sudden change in the topology between the two normal planes (B) and (NB). In particular, there is no planar symmetry as it would be expected for a configurations without technological details (i.e. with the sole smooth main stage and boosters). Finally, a jet penetration can be defined near the struts in plane (B) by the local areas of positive values of the streamwise velocity which can be clearly seen in the vicinity of the backflow area. This zone develops over a distance approximately equal to a quarter of the extension diameter ($\sim 0.25D$).

Let us be reminded that a very good agreement has been obtained between experimental and numerical values from NLR's experiments¹⁰ and ZDES calculations, respectively as shown in Weiss and Deck.^{30,32} Numerical values of $C_{p_{rms}}$ have been integrated in the frequency range used in the experiments (i.e. $St_D \in [0, 2.2]$) which is a mandatory post-processing step to properly compare both datasets. Indeed, the numerical simulation allows to obtain higher frequencies namely $St_D \in [2.2, 40]$ whose related energy cannot be neglected and leads to an offset in the azimuthal distribution of the fluctuating pressure. As for C_p values, the maxima have been observed at azimuthal locations $\Phi = 75^\circ$ and $\Phi = 260^\circ$.

These observations confirm that the aforementioned solid rotation of the flow is the main characteristic phenomenon of the flow dynamics at stake. This phenomenon can be attributed to the asymmetric struts given it was previously evidenced by Weiss and Deck³¹ on a configuration with these sole technological details. It was particularly visible in a longitudinal cut plane between an EAP and the EPC for the fluctuating $C_{p_{rms}}$ pressure coefficient comparing a three-body configuration (i.e. two boosters and a main stage) with and without struts. Such a phenomenon is still clearly visible in figures 6, 7 and 8 in the present case of a modelling using an immersed boundary method.

4.3 Step 3: assessment and validation of the side loads

The final purpose of the study is to examine the side loads using a direct integration of the pressure field on the nozzle based on the following definition of the corresponding force:

$$\vec{F}(t) = \int_0^{2\pi} \int_0^L p(x, \varphi, t) r(x) \vec{n} dx d\varphi \quad (1)$$

TOWARDS AN EFFICIENT AND ROBUST NUMERICAL STRATEGY FOR FAST AERODYNAMIC PERFORMANCE PREDICTION ON LAUNCH VEHICLES

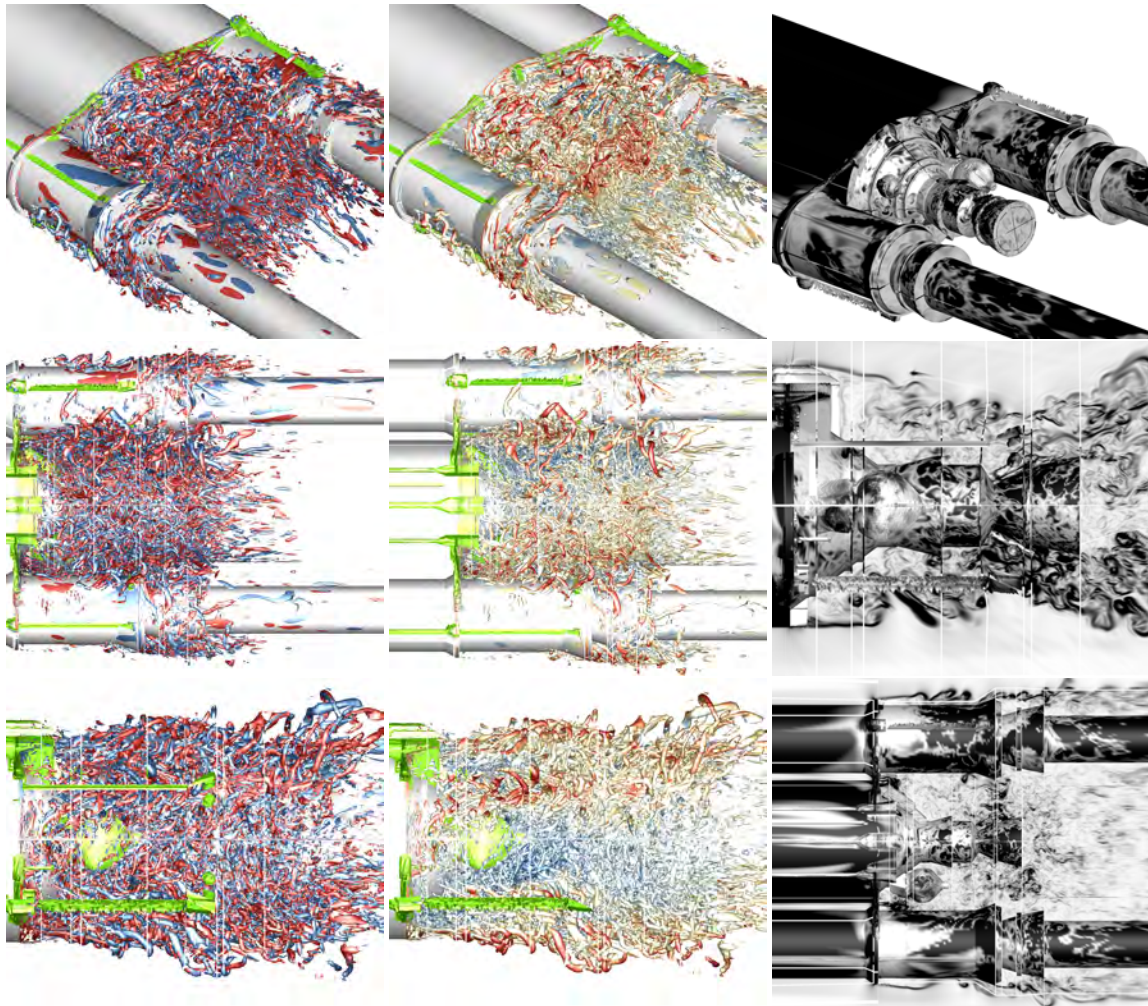


Figure 2: Visualizations of the coherent structures by means of an iso-surface $Q.U_\infty^2/D^2 = 200$ downstream the complete Ariane 5 configuration ($M_\infty = 0.8 - L/D = 1.2$). Left: coloured by the sign of the streamwise vorticity component (**red** for the positive values and **blue** for negative ones), Middle: coloured by the dimensionless streamwise velocity u/U_∞ . Right: Numerical schlieren of the instantaneous flow field at the wall and in two normal longitudinal cuts. From top to bottom: three-quarter view - $(x - z)$ plane - $(x - y)$ plane.

TOWARDS AN EFFICIENT AND ROBUST NUMERICAL STRATEGY FOR FAST AERODYNAMIC PERFORMANCE PREDICTION ON LAUNCH VEHICLES

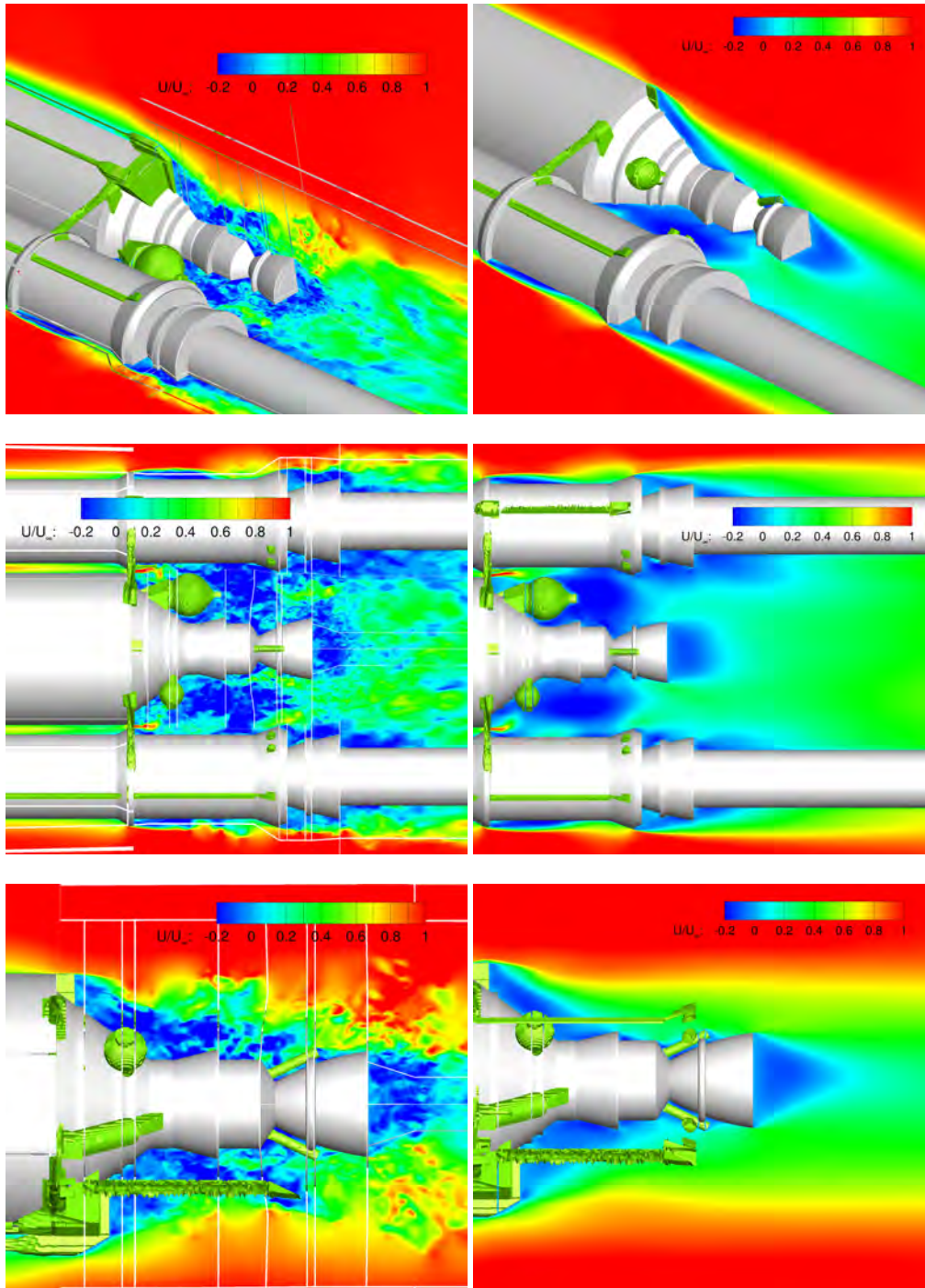


Figure 3: Iso-contours of the instantaneous u/U_∞ (left) and mean U/U_∞ streamwise velocity (right) in two orthogonal planes

TOWARDS AN EFFICIENT AND ROBUST NUMERICAL STRATEGY FOR FAST AERODYNAMIC PERFORMANCE PREDICTION ON LAUNCH VEHICLES

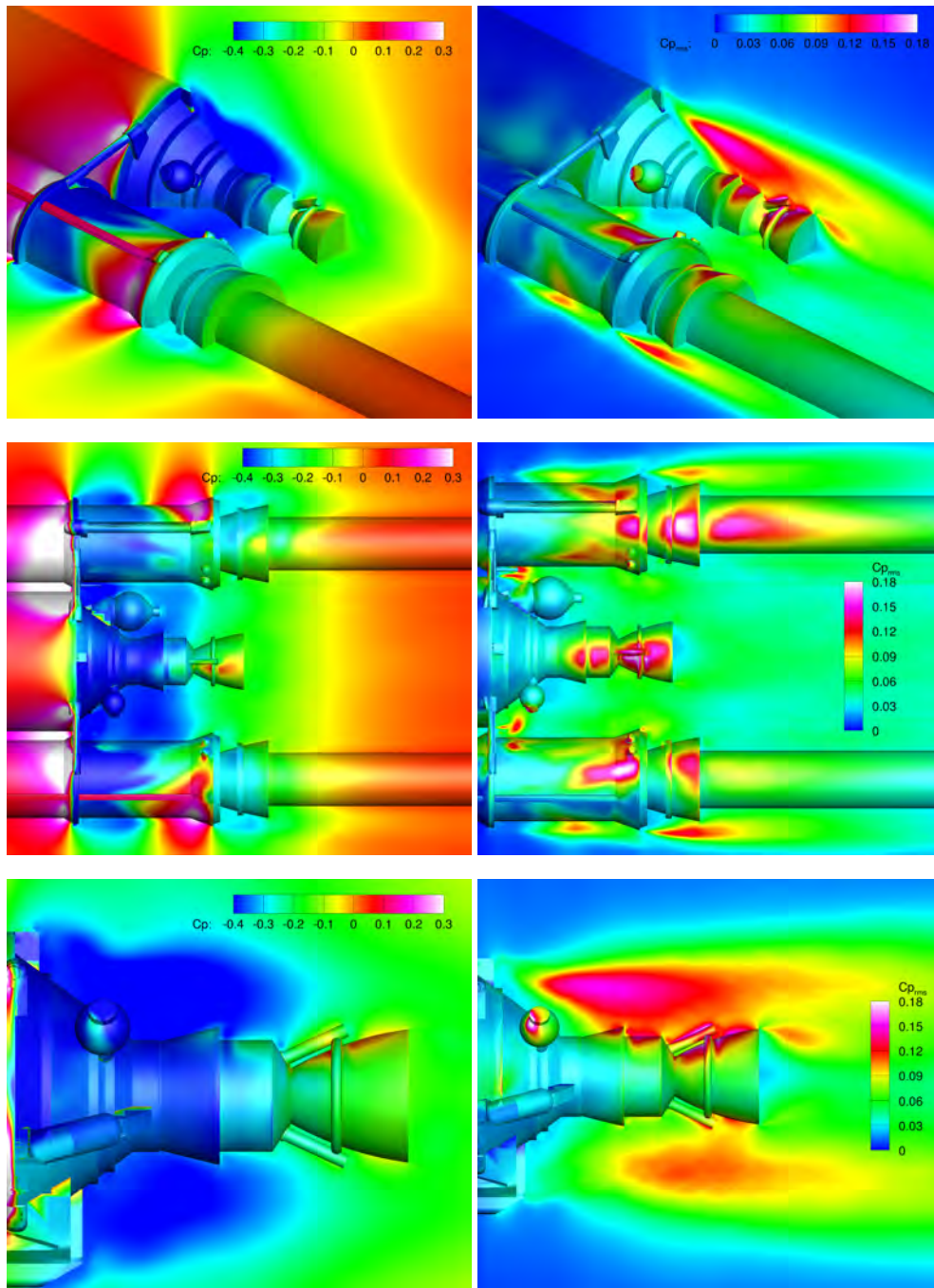


Figure 4: Mean (left) and fluctuating (right) pressure coefficient at the wall and in the flow field in two cut planes (aligned with the boosters and normal to them)

TOWARDS AN EFFICIENT AND ROBUST NUMERICAL STRATEGY FOR FAST AERODYNAMIC PERFORMANCE PREDICTION ON LAUNCH VEHICLES

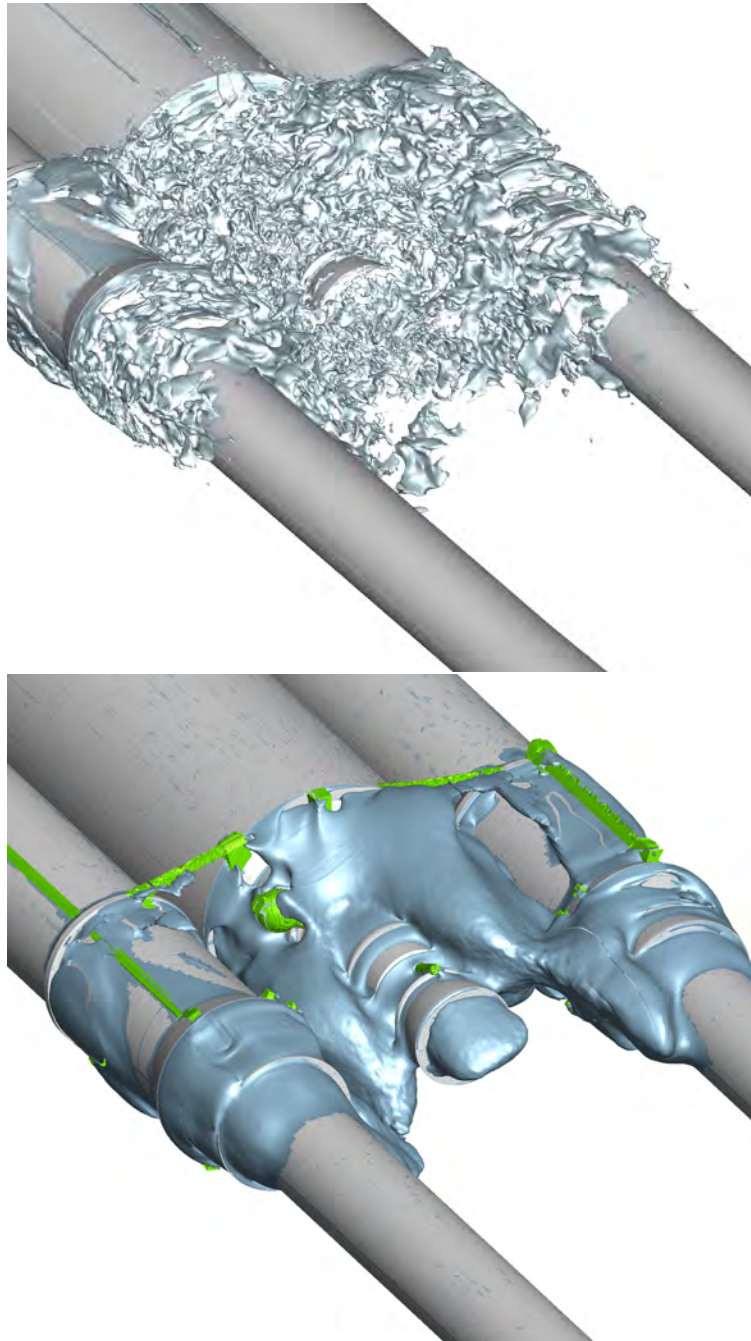


Figure 5: Iso-surface of the zero streamwise velocity $u/U_\infty = 0$. Upper part: instantaneous iso-surface - Lower part: mean iso-surface

TOWARDS AN EFFICIENT AND ROBUST NUMERICAL STRATEGY FOR FAST AERODYNAMIC PERFORMANCE PREDICTION ON LAUNCH VEHICLES

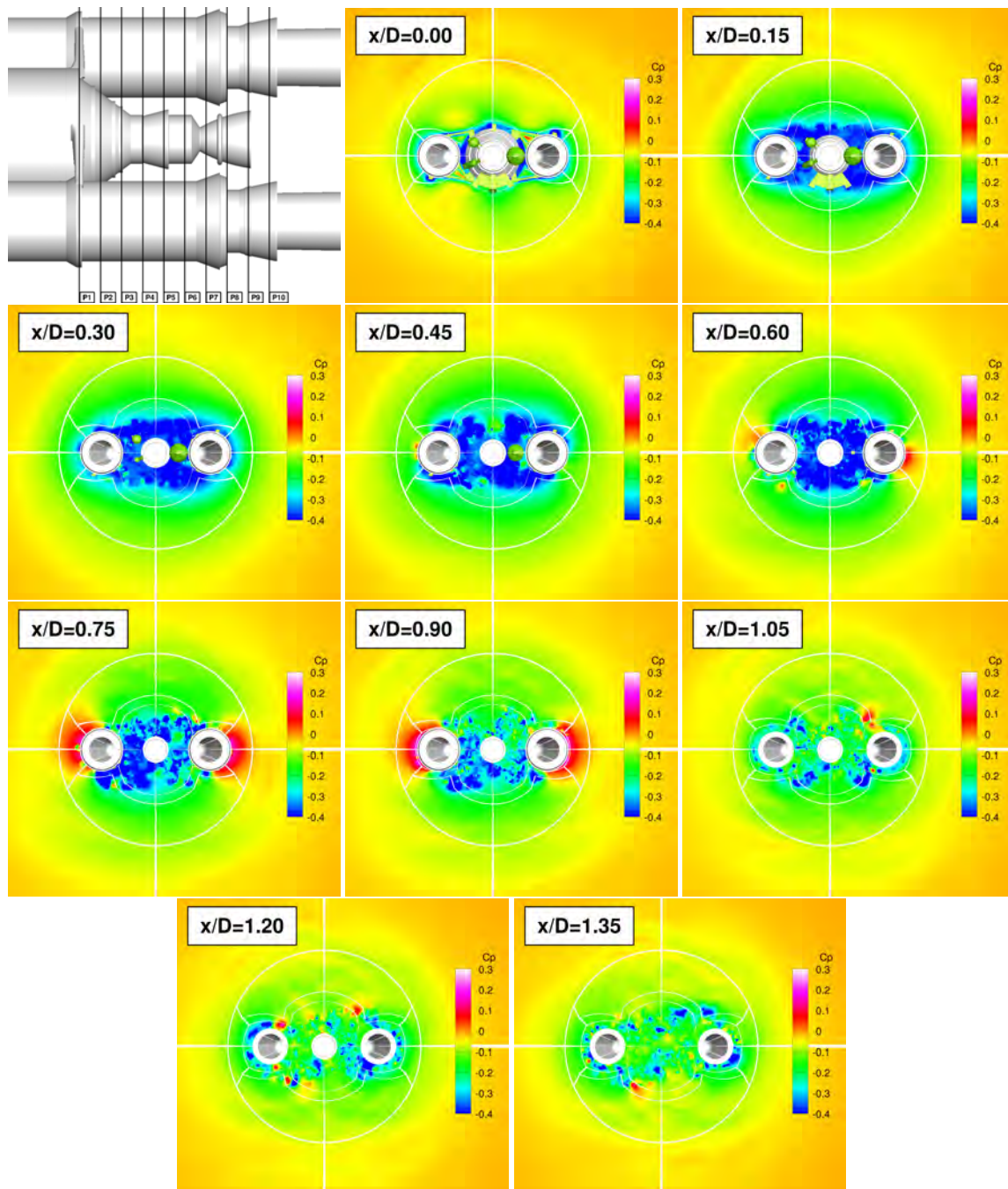


Figure 6: ($y - z$) cut planes normal to the boosters located at 10 equally distributed locations along the extension of the central part of the afterbody and coloured by the instantaneous pressure coefficient levels

TOWARDS AN EFFICIENT AND ROBUST NUMERICAL STRATEGY FOR FAST AERODYNAMIC PERFORMANCE PREDICTION ON LAUNCH VEHICLES

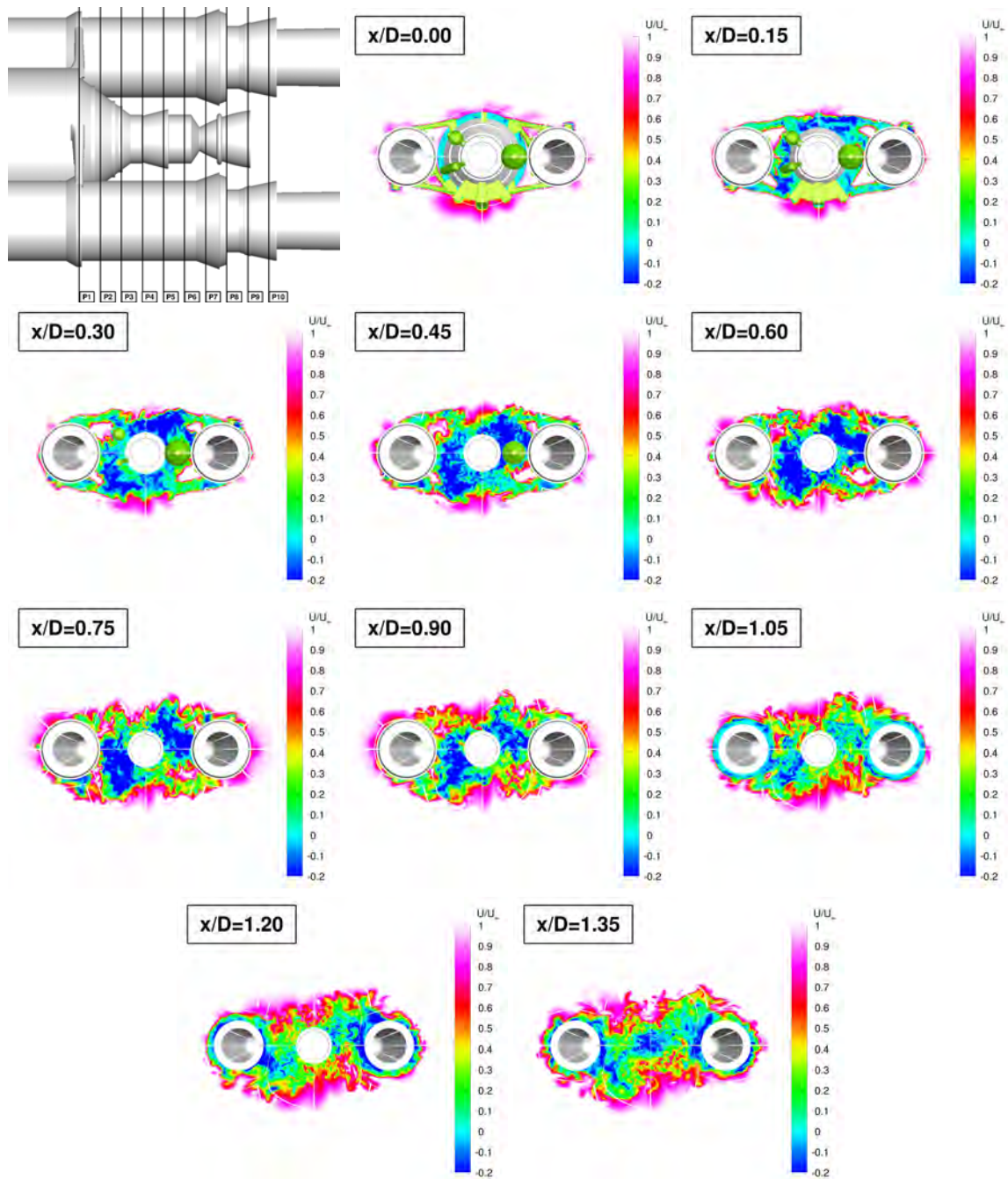


Figure 7: ($y - z$) cut planes normal to the boosters located at 10 equally distributed locations along the extension of the central part of the afterbody and coloured by the instantaneous dimensionless streamwise velocity levels

TOWARDS AN EFFICIENT AND ROBUST NUMERICAL STRATEGY FOR FAST AERODYNAMIC PERFORMANCE PREDICTION ON LAUNCH VEHICLES

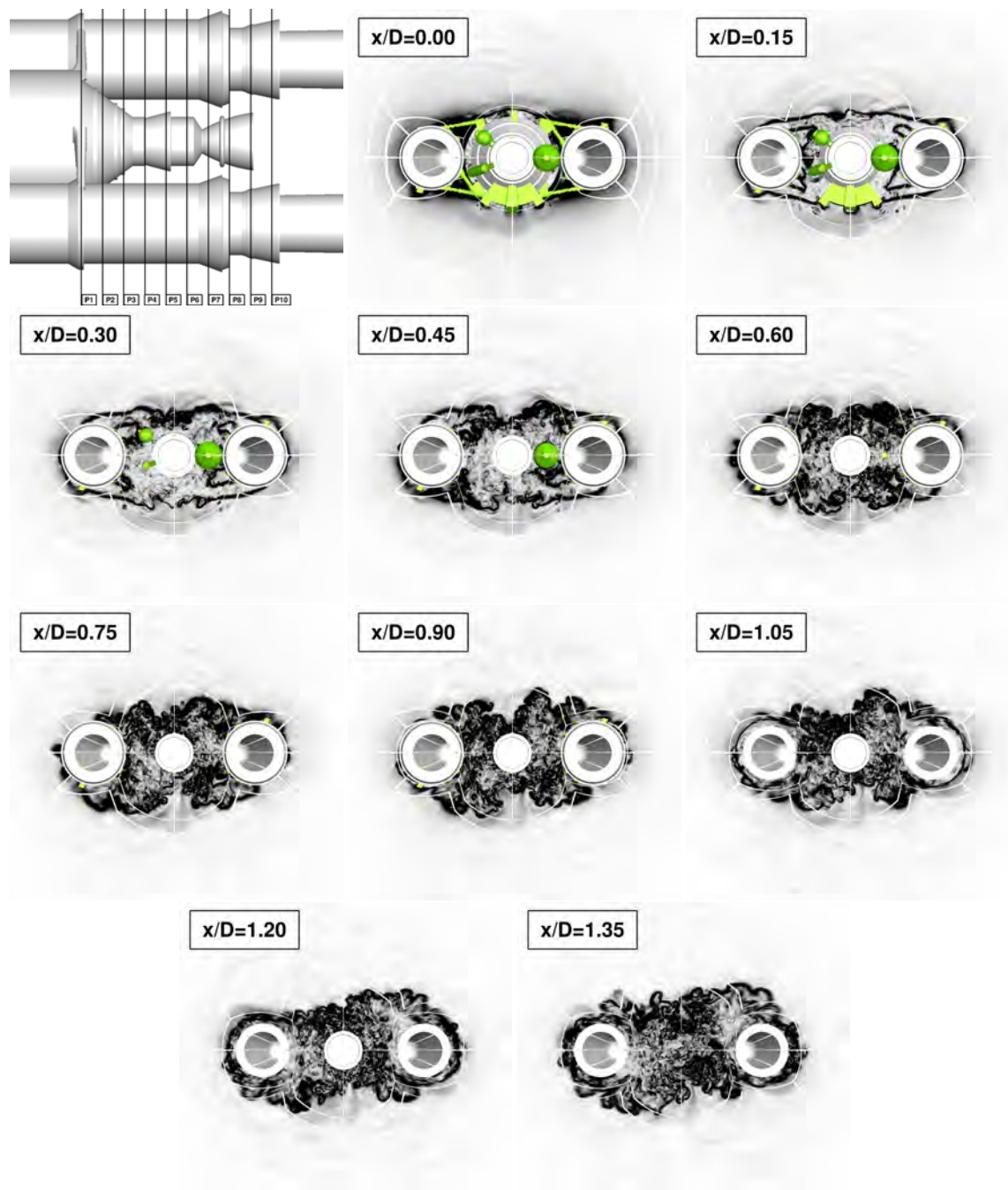


Figure 8: (y - z) cut planes normal to the boosters located at 10 equally distributed locations along the extension of the central part of the afterbody and coloured by the density gradient norm levels

TOWARDS AN EFFICIENT AND ROBUST NUMERICAL STRATEGY FOR FAST AERODYNAMIC PERFORMANCE PREDICTION ON LAUNCH VEHICLES

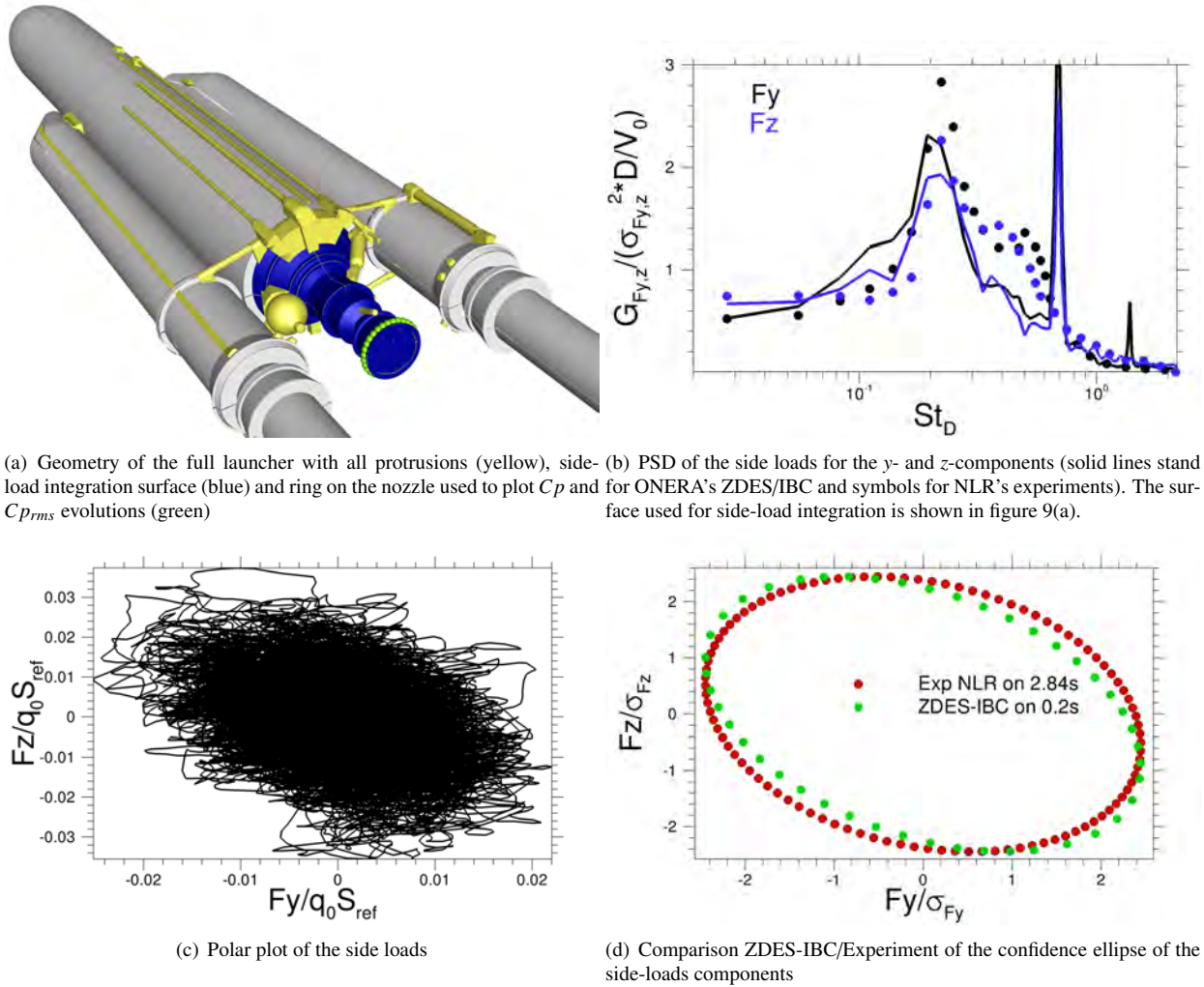


Figure 9: Assessment and validation of the side loads predicted by the ZIBC strategy

where L , $r(x)$, φ stand for the length, the nozzle radius and the azimuthal location on a ring, respectively.

The spectra of the two normal components of the load F_y and F_z (see figure 9(b)) are performed on the maximum common duration which can be defined for both the simulation and the experiments namely 0.2 s. Given the level of the statistical fluctuations observed for the peak related to the vortex shedding frequency varying in the interval $St_D \in [0.2, 0.27]$, the agreement between the ZIBC simulation and NLR's experiments appears to be very good. The combined ZDES/IBC approach permits to properly reproduce the broadband spectrum of the side loads integrated along the extension of the central part of the afterbody.

To go further into the investigation of the spectral content, the statistical properties of the effort can be described using its randomness. The side load components F_y and F_z are made dimensionless with the dynamic pressure q_0 and the reference surface $S_{ref} = \pi(D^2/4)$ based on the EPC diameter. The properties of the load components are then examined considering the bidimensional random variable $\vec{F} = (F_y, F_z)^t$ with its time average $\vec{M} = (\overline{F_y}, \overline{F_z})^t$ and its covariance matrix $C = E[\vec{F}\vec{F}^t] - \vec{M}\vec{M}^t$. The determinant of C is assumed to be equal to zero. The confidence ellipse with the confidence level $\alpha = 0.95$ containing 95% of the observations of $\vec{F}(t)$ is defined according to the border of the plane \mathbb{R}^2 determined by equation 2 (see⁶):

$$(\vec{F} - \vec{M})^t C^{-1} (\vec{F} - \vec{M}) = 2 \log(1 - \alpha) \quad (2)$$

This confidence ellipse allows to quantify the load isotropy as shown in 9(d). Let us be reminded that for an axisymmetric configuration where $\overline{F_y^2} = \overline{F_z^2}$, this ellipse becomes a circle. In figure 9(d), the sensitivity of the experimental signal duration is recalled plotting a confidence ellipse for durations similar to the simulation. To do so, the total duration of the experimental signal which is equal to 2.84 s is divided into 0.2 second long signals. For these 0.2 second long signals, the rms fluctuations of the experimental side loads are of the order of 10%.

The struts lead to a specific orientation of the loads which is more substantial in the booster plane. This ellipse is well reproduced by the ZIBC strategy.

5. Conclusion

In this paper, the milestones of an automatable strategy for accurate aerodynamic performance predictions have been detailed. It has been shown that the Zonal Immersed Boundary Conditions allow to model in a fast and efficient manner a wide variety of configurations with numerous technological details preserving the accuracy and the robustness provided by the use of a finite-volume approach computed on a simple body-fitted structured grid. In practice, the simplest elements of a given configuration are discretized in a classical body-fitted manner whereas protrusions are taken into account using a tagging procedure. Such a strategy permits to preserve most of the ZDES grid requirements and can constitute a way to perform on-demand unsteady numerical simulations with variations on the locations, shape and number of the technological details assessed.

For the side-load analysis, a 3-step study has been proposed to quantify the effort exerted on the main stage afterbody and explain its origin. First, the identification of the main instantaneous and statistical features of the flow leads to the conclusion of a pronounced asymmetry of the recirculation zone. Secondly, this asymmetry is related to a solid rotation of the global afterbody flow generating side forces acting normally to the thrust direction. Finally, the side loads have been assessed and the dimensionless values have been validated and found to be in a very good agreement with the available NLR's experimental data.

To conclude, given the simple steps necessary to build a numerical simulation workflow and the level of validation obtained regarding the loads, the Zonal Immersed Boundary Conditions (ZIBC) constitute an efficient and robust numerical strategy for fast aerodynamic performance predictions, especially on launch vehicles.

6. Acknowledgments

The Centre National d'Etudes Spatiales (CNES) is particularly acknowledged for funding the numerical activities related to the afterbody cases with struts and with all technological details modelled using IBC. The authors also thank ESA for financial support in the frame of the ESA Technology Research Programme 'Unsteady Subscale Force Measurements Within a Launch Vehicle Base Buffeting Domain' whose 'clean' afterbody mesh is used in the ZIBC approach developed in the frame of the research project ALLIGATOR funded by ONERA.

References

- [1] C. Benoit, S. Péron, and S. Landier. Cassiopee: a CFD pre- and post-processing tool. *Aerospace Science and Technology*, 45:272–243, 2015.
- [2] L. Cambier, S. Heib, and S. Plot. The Onera elsA CFD Software: Input from Research and Feedback from Industry. *Mechanics and Industry*, 14(3):159174, 2013.
- [3] F. Chalot, V. Levasseur, M. Mallet, G. Petit, and N. Reau. LES and DES Simulations for Aircraft Design. *45th AIAA Aerospace Sciences Meeting and Exhibit, AIAA Paper*, (2007-0723), 2007.
- [4] S. Deck. Zonal-Detached-Eddy Simulation of the flow around a high-lift configuration. *AIAA Journal*, 43(11):2372–2384, November 2005.
- [5] S. Deck. Recent improvements in the Zonal Detached Eddy Simulation (ZDES) formulation. *Theoretical and Computational Fluid Dynamics*, 26(6):523–550, December 2012.
- [6] S. Deck and A.T. Nguyen. Unsteady side-loads in a thrust-optimized contour nozzle at hysteresis regime. *AIAA Journal*, 42(9):1878–1888, September 2004.
- [7] S. Deck and P. Thorigny. Unsteadiness of an axisymmetric separating-reattaching flow. *Physics of Fluids*, 19(065103), 2007.
- [8] E. A. Fadlun, R. Verzicco, P. Orlandi, and J. Mohd-Yusof. Combined immersed-boundary/finite-difference methods for three-dimensional complex flow simulations. *Journal of Computational Physics*, 161(1):35–60, 2000.

TOWARDS AN EFFICIENT AND ROBUST NUMERICAL STRATEGY FOR FAST AERODYNAMIC PERFORMANCE PREDICTION ON LAUNCH VEHICLES

- [9] E. G. M. Geurts. Steady and unsteady pressure measurements on the rear section of various configurations of the ariane 5 launch vehicle. *6th International Symposium on Launcher Technologies, Munich, Germany, November, 2005*.
- [10] E. G. M Geurts. Unsteady subscale force measurements within a launch vehicle base buffeting environment. Wind tunnel test of buffeting reduction devices (NLR-CR-2010-396 - test 7003). June 2010.
- [11] P. Guillen and M. Dormieux. Design of a 3D multi-domain Euler code. In *International Seminar of Supercomputing*, Boston, USA, 1989.
- [12] K. Hannemann, J.-F. Pallegoix, H. Lambaré, J.M. J. Maseland, M. Frey, S. Deck, F. F. J. Schrijer, and R. Schwane. Launch vehicle base buffeting: Recent experimental and numerical investigations. *Proceedings of the 7th European Symposium on Aerothermodynamics for Space Vehicles, ESA Communications, ESTEC, Noordwijk, The Netherlands*, May 2011.
- [13] S. K. Lele. Compact finite differences schemes with spectral-like resolution. *Journal of Computational Physics*, 103:16–42, 1992.
- [14] M. S. Liou. A sequel to AUSM : AUSM+. *J. Comp. Phys.*, 129:364–382, 1996.
- [15] H. Lüdeke, J.D. Mulot, and K. Hannemann. Launch Vehicle Base Flow Analysis Using Improved Delayed Detached-Eddy Simulation. *AIAA Journal*, 53:2454–2471, 2015.
- [16] S. Marie, Ph Druault, H. Lambare, and F. Schrijer. Experimental analysis of the pressure-velocity correlations of external unsteady flow over rocket launchers. *Aerospace Science and Technology*, 30(1):83–93, October 2013.
- [17] I. Mary and P. Sagaut. Large eddy simulation of flow around an airfoil near stall. *AIAA J.*, 40(6):1139, jun 2002.
- [18] L. Mochel, P. E. Weiss, and S. Deck. Zonal Immersed Boundary Conditions: Application to a high Reynolds number afterbody flow. *AIAA Journal*, 52(12):2782–2794, 2014.
- [19] J. Mohd-Yusof. Combined immersed-boundary/b-spline methods for simulations of flows in complex geometries. *Annual Research Briefs, Center for Turbulence Research*, page 317328, 1997.
- [20] R. Pain, P. E. Weiss, and S. Deck. Zonal Detached Eddy Simulation of the flow around a simplified launcher afterbody. *AIAA Journal*, 52:1967–1979, 2014.
- [21] M. Péchier, P. Guillen, and R. Caysac. Magnus effect over finned projectiles. *AIAA Journal of Spacecraft and Rockets*, 38(4):542–549, 2001.
- [22] A. Roux, S. Reichstadt, N. Bertier, L. Gicquel, F. Vuillot, and T. Poinso. Comparison of Numerical Methods and Combustion Models for LES of a Ramjet. *Combustion for Aerospace Propulsion*, 337(6-7):313572, 2009.
- [23] F. F. J. Schrijer, A. Sciacchitano, and F. Scarano. Spatio-temporal and modal analysis of unsteady fluctuations in a high-subsonic base flow. *Physics of Fluids*, 26(8), August 2014.
- [24] R. Schwane. Numerical Prediction and Experimental Validation of Unsteady Loads on ARIANE 5 and VEGA. *Journal of Spacecraft and Rockets*, 52:54–62, 2015.
- [25] F. Simon, S. Deck, P. Guillen, P. Sagaut, and A. Merlen. Numerical simulation of the compressible mixing layer past an axisymmetric trailing edge. *Journal of Fluid Mechanics*, 591:215–253, 2007.
- [26] V. Statnikov and Schröder W. Meinke, M. Reduced-order analysis of buffet flow of space launchers. *Journal of Fluid Mechanics*, 815:1–25, 2017.
- [27] F. Vuillot, F. Houssen, E. Manoha, S. Redonnet, and J. Jacob. Applications of the CEDRE Unstructured Flow Solver to Landing Gear Unsteady Flow and Noise Predictions. *17th AIAA/CEAS Aeroacoustics Conference, AIAA Paper*, (2011-2944), 2011.
- [28] P. E. Weiss and S. Deck. Control of the antisymmetric mode ($m=1$) for high reynolds axisymmetric turbulent separating/reattaching flows. *Physics of Fluids*, 23:095102, 2011.
- [29] P. E. Weiss and S. Deck. Numerical investigation of the robustness of an axisymmetric separating/reattaching flow to an external perturbation using ZDES. *Flow Turbulence & Combustion*, 91:687–715, 2013.

TOWARDS AN EFFICIENT AND ROBUST NUMERICAL STRATEGY FOR FAST AERODYNAMIC PERFORMANCE
PREDICTION ON LAUNCH VEHICLES

- [30] P. E. Weiss and S. Deck. On the coupling of a zonal body-fitted/immersed boundary method with zdes: application to the interactions in a full space launcher afterbody flow. *4th International Conference on Turbulence and Interactions*, 2015.
- [31] P. E. Weiss and S. Deck. ZDES of the flow dynamics on an Ariane 5-type afterbody with and without struts. *6th European Conference for Aerospace Sciences, Flight Physics, Launcher Aerodynamics*, 2015.
- [32] P. E. Weiss and S. Deck. On the coupling of a zonal body-fitted/immersed boundary method with zdes: application to the interactions on a realistic space launcher, revised. *Computers and Fluids*, 2017.
- [33] P. E. Weiss, S. Deck, J. C. Robinet, and P. Sagaut. On the dynamics of axisymmetric turbulent separating/reattaching flows. *Physics of Fluids*, 21(075103), 2009.